ELSEVIER

Journal of Nuclear Materials 258–263 (1998) 1380–1385

journal of nuclear materials

Microstructural examination of irradiated V–(4–5%)Cr–(4–5%)Ti

D.S. Gelles [a,*,1], P.M. Rice [b], S.J. Zinkle [b], H.M. Chung [c]

[a] *Pacific Northwest National Laboratory, MS P8-15, P.O. Box 999, Richland, WA 99352, USA*
[b] *Oak Ridge National Laboratory, Oak Ridge, TN 37831-6376, USA*
[c] *Argonne National Laboratory, Argonne, IL 60439, USA*

Abstract

Microstructural examination results are reported for two heats of V–(4–5%)Cr–(4–5%)Ti irradiated in the EBR-II X530 experiment to 4.5 dpa at ~400°C to provide an understanding of the microstructural evolution that may be associated with degradation of mechanical properties. Fine precipitates were observed in high density intermixed with small defect clusters for all conditions examined following the irradiation. The irradiation-induced precipitation does not appear to be affected by preirradiation heat treatment at 950–1125°C. There was no evidence for a significant density of large (diameter > 10 nm) dislocation loops or network dislocations. Analytical investigations successfully demonstrated that the precipitates were enriched in titanium, depleted in vanadium and contained no nitrogen. These results are discussed in terms of future alloy development options.

1. Introduction

Vanadium-based alloys are being developed for application as a first wall material for magnetic fusion power systems. It has been shown that alloys of composition V–(4–5%)Cr–(4–5%)Ti have very promising physical and mechanical properties [1]. Recent attention in this alloy class has focused on several issues, such as the effect of low-temperature irradiation on fracture toughness, the effect of helium generation, the effect of minor impurities, and heat-to-heat variation in work-hardening behavior at low irradiation temperatures. While other classes of alloys are still considered, it may still be possible to optimize the V–(4–5%)Cr–(4–5%)Ti alloys in order to suppress their susceptibility to loss of work-hardening capability following irradiation at low temperatures. Susceptibility of the alloy class to this process under fusion-relevant helium-generating conditions is considered to be a major factor in governing the minimum operating temperature of magnetic fusion devices.

Recent irradiation experiments at <430°C have shown that the loss of work-hardening capability and uniform elongation of V–4Cr–4Ti vary strongly from heat to heat and are influenced significantly by helium generated in the alloy [2]. The present effort was initiated to provide an understanding of the microstructural evolution in some heats of the V–(4–5%)Cr–(4–5%)Ti class that correspond to specimens with degradation of mechanical properties [3]. Specifically, two issues were addressed: the microstructural characteristics of a 500-kg heat of V–4Cr–4Ti (Heat #832665, referred to in Ref. [3] as BL-71) not previously examined following irradiation, and the cause of degraded properties in both an 80-kg heat of V–5Cr–5Ti (Heat BL-63) and the 500-kg heat following irradiation at ~385°C to ~4 dpa in the X530 experiment in the Experimental Breeder Reactor - II (EBR-II). Finally, it can be noted that whereas the 500-kg heat did suffer from virtual loss of work-hardening capability during the irradiation, samples of a Russian 100-kg heat of V–4Cr–4Ti (Heat VX-8) gave widely varying results depending on the irradiation capsule, indicating that irradiation induced hardening may be avoided [4].

* Corresponding author. Tel.: +1 509 376 3141; fax: +1 509 376 0418; e-mail: ds_gelles@pnl.gov.

[1] Operated for the US Department of Energy by Battelle Memorial Institute under Contract DE-AC06-76RLO 1830.

0022-3115/98/$19.00
PII: S0022-3115(98)00206-2

2. Experimental procedure

Specimens in the form of microscopy disks 3 mm in diameter were included in the X530 experiment. Five samples were selected for examination comprising two heats of material but each with a different preirradiation heat treatment condition. The compositions of the heats are given in Table 1 [5,6] and the specimen conditions are shown in Table 2. Specimens of BL-63 had been included in capsule S8 and specimens of BL-71 had been included in capsule S9 of the EBR-II X530 experiment [7] which achieved an exposure of 35 effective full power days yielding a peak fluence of 7.3×10^{21} n/cm^2 ($E > 0.1$ MeV) corresponding to damage of ~4 dpa [8]. The capsules also contained matching miniature tensile specimens of the same conditions but from thicker sheet stock. The bottom of capsule S8 was 9.80 in. from the bottom of the core and the bottom of capsule S9 was 7.35 in. above the bottom of the core upon which actual irradiation temperatures and doses have been estimated and included in Table 2 [9,10]. One specimen of each of the BL-71 conditions was electrolytically thinned at ANL following irradiation, and one specimen of each of the BL-63 conditions was thinned at PNNL. Specimen BL-71-WR1050 was briefly repolished at PNNL. Examinations were performed on JEOL 1200EX and 2010F analytical transmission microscopes at PNNL and on Philips CM12 and CM200 microscopes at ORNL.

3. Results

The microstructures of all conditions were as expected, showing large and intermediate sized (Ti,V) oxy-carbo-nitride particles randomly distributed, and small particles decorating grain boundaries in the BL-71-WR1050 and BL-71-WR1125 [11]. Evidence for effects of irradiation could only be identified on a fine scale but was quite apparent at magnifications on the order of 30KX.

Careful examination of diffraction information indicated enhanced scattering in two regions of reciprocal space: a radial streak in the $\langle 2\ 0\ 0 \rangle$ direction at approximately 3/4 $\langle 2\ 0\ 0 \rangle$ and a similar tangential streak at approximately 2/3 $\langle 2\ 2\ 2 \rangle$. Dark field imaging with each of these features showed similar but not identical distributions of fine features, assumed to be precipitates. As streaking is in different directions for each of these diffraction features, different populations of precipitates would be expected to be in contrast. Similar attempts to image the dislocation structure using weak beam conditions on matrix reflections gave very complex images with features of similar size to the precipitate features. It is therefore likely that several matrix reflections superimpose on precipitate reflections. It was possible to obtain precipitate dark field images for each sample condition using 3/4 $\langle 2\ 0\ 0 \rangle$ contrast in stereo by tilting on (2 0 0). Stereo model observations demonstrated that the precipitate features tended to form in layers distributed through the foil thickness, verifying that they were not surface artifacts. All specimens gave similar diffraction behavior. Examples of one dark field image for each sample condition using $\vec{g} = 3/4\ \langle 2\ 0\ 0 \rangle$ are provided in Fig. 1. Fig. 1 also includes an example of the diffraction information, inset.

From Fig. 1, it can be seen that precipitation is very fine. For example, particles in Fig. 1(d) are 2 nm long by 1 nm wide, the narrow dimension corresponding to the streaking in $\langle 2\ 0\ 0 \rangle$. It is surprising that such small particles can be successfully imaged. The precipitate dark field images appear to differ between the two heats,

Table 1
Composition of heats examined

Heat #	Nominal composition, (wt%)	Minor impurities (wppm)				
		O	N	C	Si	Other
BL-63	V–4.6Cr–5.1Ti	440	28	73	310	200 Al
832665, BL-71	V–3.8Cr–3.9Ti	310	85	80	783	220 Fe, 190 Al

Table 2
Specimen and irradiation conditions for the X530 experiment

Specimen designation	Preirradiation heat treatment	Fluence (n/cm^2)	Dose (dpa)	Temperature (°C)
BL-63-CR950	Cold rolled, annealed at 950°C/1 h	6.7×10^{21}	4.3	400
BL-63-CR1050	Cold rolled, annealed at 1050°C/1 h	6.7×10^{21}	4.3	400
BL-71-WR950	Warm rolled, annealed at 950°C/1 h	7.3×10^{21}	4.7	400
BL-71-WR1050	Warm rolled, annealed at 1050°C/1 h	7.3×10^{21}	4.7	400
BL-71-WR1125	Warm rolled, annealed at 1125°C/1 h	7.3×10^{21}	4.7	400

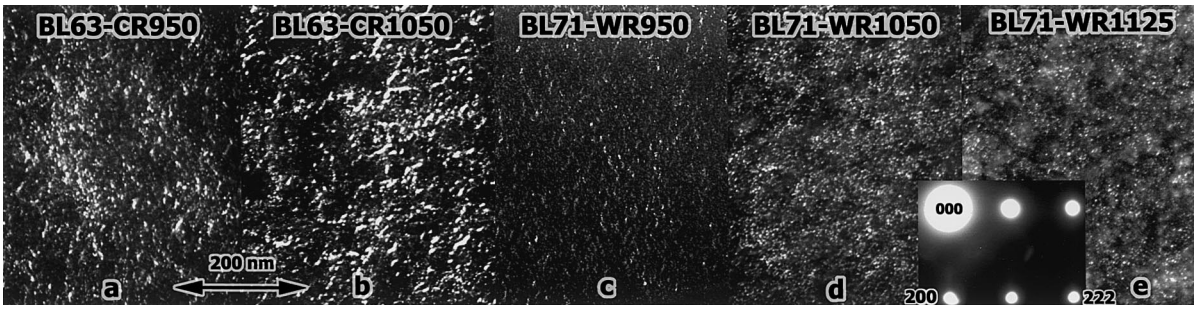

Fig. 1. Precipitate dark field images for specimens of V–(4–5%)Cr–(4–5%)Ti irradiated in the X530 experiment with a (0 1 1) diffraction pattern from BL-71-WR1125 inset.

but the size distribution is invariant with respect to the preirradiation heat treatment. The exact nature of the differences between the precipitate morphologies for the two heats is difficult to quantify. Although the images of precipitates in BL-63 appear to be larger, careful examination of the negatives suggests that the larger particles are a result of rafts of closely spaced smaller particles, of similar size to those in BL-71. However, it can be argued that the particles are larger in BL-63, and the fine structure appears for other reasons. The precipitation response made imaging the dislocation structure impractical. Neither defect clusters (dislocation loops) or network dislocations were successfully imaged.

Stereoscopic precipitate measurements gave particle densities as follows; BL-63-CR950: 6.3 nm mean diameter at 4×10^{17} cm^{-3} for a volume fraction of 3.5%, BL-63-CR1050: 4.9 nm mean diameter at 2×10^{17} cm^{-3} for a volume fraction of 0.8%, BL-71-WR950: 4.4 nm mean diameter at 1.1×10^{17} cm^{-3} for a volume fraction of 0.3%, BL-71-WR1050: 4.8 nm mean diameter at 4×10^{17} cm^{-3} for a volume fraction of 1.3%, and BL-71-WR1125: 3.7 nm mean diameter at 3×10^{17} cm^{-3} for a volume fraction of 0.4%. These measurements should be considered estimates given the difficulty of the analysis, but they provide further indication that the precipitation found could be responsible for the observed irradiation hardening in BL-71 but do not explain the difference in behavior between the two heats.

Several attempts were made to obtain compositional information from the fine precipitate features using energy dispersive X-ray spectroscopy EDS. Difficulties were encountered identifying the exact location of a

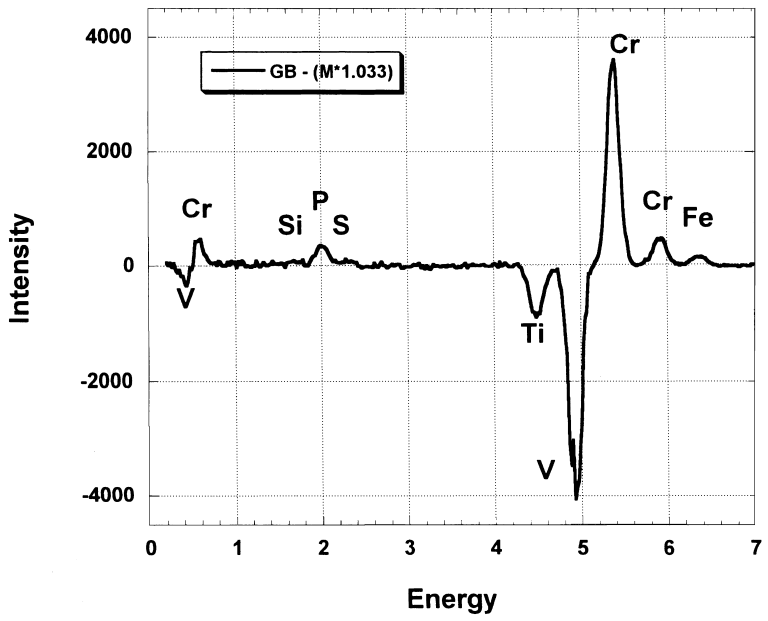

Fig. 2. Grain boundary EDX difference spectrum showing chromium enrichment following irradiation in the X530 experiment.

precipitate so that a 1 nm focussed spot could be positioned to obtain characteristic precipitate composition information. Techniques based on 3/4 ⟨2 0 0⟩ dark field imaging and lattice imaging to identify precipitate locations failed to provide any composition dependencies that could be considered characteristic. Initial attempts to identify composition differences at a grain boundary in BL-71-WR1050 were also unsuccessful.

Improved reliability was achieved by computer-controlled beam placement on precipitates or matrix regions (spot or line profiles) using annular dark field (ADF) STEM images with the aid of an Emispec system. A total of seven sets of spot profiles were taken at different grain boundary regions and in the matrix, avoiding regions containing precipitates. The matrix and grain boundary energy dispersive X ray spectroscopy (EDS) profiles were normalized using the background signal at positions well-separated from spectrum peaks (2.5–4 keV and 8–12 keV energies). As indicated in Fig. 2, the difference between the resultant normalized profiles showed a strong amount of Cr enrichment and corresponding V depletion at the irradiated grain boundary compared to the matrix composition. The grain boundary also showed a slight depletion of Ti and enrichment of P and Fe. Chromium enrichment at irradiated grain boundaries was also observed in the 500 kg heat of V–4Cr–4Ti following neutron irradiation to 0.5 dpa at 420°C [12]. It should be noted that significant Ti enrichment (with V depletion) was observed at grain boundaries in the unirradiated alloy after annealing for 1 h at 1000°C.

The matrix precipitate composition was studied in more detail using an ADF aperture and a Parallel Electron Energy Loss Spectrometer (PEELS). A PEELS line profile showing Ti concentrations varying across the specimen which correlates with defects as imaged by ADF scanning transmission electron microscopy is shown in Fig. 3. This titanium signal has been enhanced by dividing by the vanadium signal. A 100 eV window in front of the L edge was used to fit, extrapolate and subtract a background from the EELS spectra below the titanium L edges. The beam trace is defined by the 50 nm line across the micrograph insert. An good fit between enhanced titanium concentrations and bright features in the dark field image was obtained.

The Ti/V ratio plotted in Fig. 3 is of a qualitative nature only intended to show that the peaks in Ti concentration correlate well with the defects visible in the STEM images. The ratio was plotted since it automatically corrects for thickness and diffraction effects. It should not be considered a plot of quantitative values. It can be noted that the peaks in Ti concentration correlate well, but not perfectly, with the intensity in the ADF STEM image. The line profile crossed four bright defects, all of which correspond to a peak in Ti intensity, but between the last two defects the profile shows another peak in Ti concentration where no defect is visible.

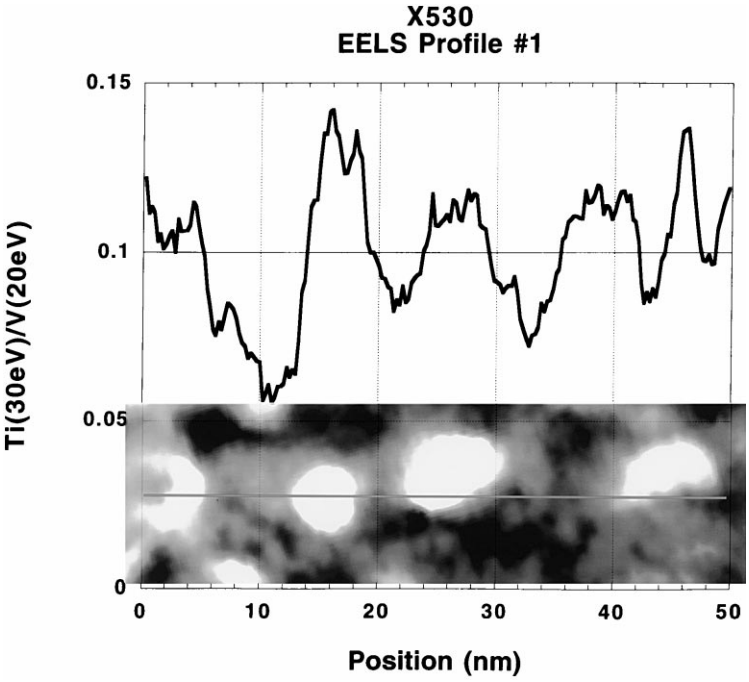

Fig. 3. Titanium vanadium ratio based on a PEELS Line Profile across defects visible in ADF STEM mode with the corresponding 50 nm beam trace marked on the micrograph inset.

This may be due to the presence of several variants in orientation so that not all appear in the same dark field image.

4. Discussion

The purpose of this work was to provide an explanation for mechanical property degradation in two heats of V–(4–5%)Cr–(4–5%)Ti. The above results indicate that precipitation during irradiation is responsible for irradiation hardening. Unfortunately, the composition of the precipitate has not yet been completely established, so that it is not yet possible to provide recommendations for composition modifications for improved properties. This discussion is provided as speculation on the likely causes for the behavior observed.

Several important facts should be first summarized. Table 3 provides postirradiation mechanical properties response [3] for conditions identical to those examined in this study. From Table 3, it can be shown that BL-63 gave lower levels of both yield strength (YS) and ultimate tensile strength (UTS), but uniform elongation (UE) was similar in comparison with BL-71 following annealing at 950°C, whereas higher annealing temperatures for BL-71 produced lower UE. Total elongation (TE) values followed none of these trends. These properties corresponded to ductile to brittle transition temperatures (DBTTs) >300°C. Therefore, to a first order, both alloys have unacceptable properties following irradiation at low temperatures. However, comparison of the compositional differences in Table 1 demonstrates that BL-71 contains less chromium and titanium but higher silicon.

Therefore, the experimental observations can be summarized as follows. BL-71 develops more hardening and less uniform elongation following irradiation; BL-71 contains significantly more silicon and a little less chromium and titanium, but the irradiation temperatures are expected to be very similar [9]. However, it should be noted that all of the specimens in subcapsule S9 (including BL-71) exhibited lower tensile ductilities than specimens irradiated in subcapsule S8. Based on this, one likely cause for the observed enhanced hardening would be expected to be precipitation of silicide phases. The observed precipitate particles are very finely distributed, and precipitate number density has been measured for each condition. It can be argued that the particles may be larger or more non-uniformly distributed in BL-63, and therefore effectively at lower density (although not supported by quantitative microscopy because distribution is not taken into account), in agreement with the observed hardening behavior. Another explanation may be envisioned arising from impurity transfer from the 304 stainless steel subcapsule walls.

The diffraction information obtained for this fine precipitation does not straightforwardly correspond to precipitation previously identified in this alloy class. Chung and Smith [13] have provided diffraction information for $Ti_5(Si,P)_3$ and Ti_2O that have similar appearance but different diffraction response. One published diffraction pattern in Fig. 2 of Ref. [13] does show a streak at 2/3 $\langle 2\ 2\ 2\rangle$, but no comment is provided. Chung et al. [14] found similar grain boundary contrast in V–4Cr–4Ti irradiated at 425°C to 31 dpa in the DHCE experiment but ruled out Ti_5Si_3 precipitation. Chung et al. [15] showed microstructures in irradiated V–4Cr–4Ti containing Ti_5Si_3, but provided no diffraction information. Satou et al. [16] showed diffraction and dark field images of Ti_5Si_3 precipitates in V–5Ti–5Cr–1Si–Al following irradiation at 520°C, but the diffraction information is not in agreement with the present findings. Gelles and Chung [17] found precipitation in V–5Cr–5Ti following irradiation with a diffraction streak at 3/4 $\langle 2\ 0\ 0\rangle$, but compositional information was not obtained, and it was "anticipated that the phase was TiP, but similar morphologies have been identified previously as Ti_5Si_3." Chung et al. [18] again published a grain boundary image in V–4Cr–4Ti irradiated at 425°C to 31 dpa similar to those in the present work. Finally, Fukumoto et al. [19] showed dark field images of similar features in V–4Cr–4Ti following irradiation but identified them as titanium oxide, Ti_2O or TiO_x ($x < 0.5$) without giving any diffraction information. Therefore, titanium oxide may be a reasonable but unproven identification of the irradiation hardening phase found in our work.

Table 3
Postirradiation mechanical properties for selected specimens in the X530 experiment irradiated at 400°C to 4 dpa

Specimen designation	Preirradiation heat treatment	0.2% YS (MPa)	UTS (MPa)	UE(%)	TE(%)
BL-63-CR950	Cold rolled, annealed at 950°C/1 h	701	743	0.8	2.8
BL-63-CR1050	Cold rolled, annealed at 1050°C/1 h	723	765	1.0	7.0
BL-71-WR950	Warm rolled, annealed at 950°C/1 h	819	847	0.8	4.1
BL-71-WR1050	Warm rolled, annealed at 1050°C/1 h	809	818	0.4	6.0
BL-71-WR1125	Warm rolled, annealed at 1125°C/1 h	880	883	0.2	6.0

It can also be noted that ongoing work on some heat treated welds of the V–4Cr–4Ti alloy showed very strong diffraction spots at 3/4 (2 0 0) [20]. The heat treatment results in many (1 0 0) planar precipitates which have an FCC crystal structure with $a_o = 0.428$ nm. The precipitate [1 0 0] corresponds to the Matrix [1 1 0]. The precipitate d_{200} lattice spacing matched the matrix d_{110} perfectly on two of the three axes, and thus the shape is a large-diameter, thin disk. Previous work on welds heat treated similarly showed the precipitates to be $Ti_7O_4N_2C$. Therefore, it is possible that the precipitates found following irradiation in the X530 experiment are of type Ti(OCN). It is not yet certain that the 2/3(2 2 2) diffraction spots are due to these defects; they may be due to a different set of precipitates.

From these analyses it appears that the precipitate found in the present work cannot be identified as a silicide based on diffraction information, whereas it may be, but has not definitively been shown to be, an oxide or a phosphide. If an oxy-carbo-nitride is responsible for the hardening found in the X530 experiment, then differences between the BL-63 and BL-71 alloys could best be explained by a consequence of variation in irradiation temperature in different subcapsules and not composition. However, as noted in Table 2, due to capsule radial positions, the calculated irradiation temperatures are identical [9]. A phosphide cause for embrittlement is unlikely because phosphorus levels are low in BL-71 [6]. The most critical experiment continues to be identification of the phase in BL-71 that causes the diffraction streaks at 3/4 ⟨2 0 0⟩ and 2/3 ⟨2 2 2⟩.

5. Conclusions

Five specimen conditions from the X530 experiment, comprising two heats of V–(4–5%)Cr–(4–5%)Ti given different preirradiation heat treatments and corresponding to tested mechanical properties specimens, have been examined to identify the cause of irradiation hardening. It is found that hardening is at least in part due to precipitation of a high density of small particles. However, analytical electron microscopy was unable to provide quantitative precipitate composition and it is not yet possible to provide an explanation for the differences in response between the heats.

References

[1] B.A. Loomis, A.B. Hull, D.L. Smith, J. Nucl. Mater. 179–181 (1992) 148.
[2] H.M. Chung, M.C. Billone, D.L. Smith, DOE/ER-0313/22, 1998, p. 22.
[3] S.J. Zinkle, D.J. Alexander, J.P. Robertson, L.L. Snead, A.F. Rowcliffe, L.T. Gibson, W.S. Eatherly, H. Tsai, DOE/ER-0313/21, 1997, p. 73.
[4] H.M. Chung, D.L. Smith, DOE/ER-0313/22, 1998, p. 33.
[5] H.M. Chung, J. Gazda, L.J. Nowicki, J.E. Sanecki, D.L. Smith, DOE/ER-0313/15, 1993, p. 207.
[6] H.M. Chung, H. Tsai, D.L. Smith, K. Peterson, C. Curtis, C, Wojcik, R. Kinney, DOE/ER-0313/17, 1994, p. 178.
[7] H. Tsai, V. Strain, A.G. Hins, H.M. Chung, L.J. Nowicki, D.L. Smith, DOE/ER-0313/17, 1994, p. 8.
[8] H. Tsai, V. Strain, A.G. Hins, H.M. Chung, L.J. Nowicki, D.L. Smith, DOE/ER-0313/18, 1995, p. 85.
[9] Bob Strain, ANL: A more refined thermal analysis of the X530 experiment shows that the centerline temperature for subcapsule S8 to be 400.5°C and that for S9 to be 399.1°C. The subcapsule inside surface temp was ~1.5°C lower, in both cases. S8, at a higher axial elevation, ordinarily would have a higher temperature. But the capsule it was in, AH2, was located at the center of the hex, thus receiving less heat from the neighboring (hotter) subassemblies. The two countervailing effects essentially cancelled out, personal communication.
[10] L.W. Greenwood, PNNL, recommending that an extra column be added to Table 3, DOE/ER-0313/21, 1996, p. 228, headed dpa (vanadium) and reading 14.0, 31.0, 38.1, 29.3, 15.4, 6.36, personal communication.
[11] D.S. Gelles, H. Li, DOE/ER-0313/19, p. 22.
[12] P.M. Rice, S.J. Zinkle, these Proceedings.
[13] H.M. Chung, D.L. Smith, J. Nucl. Mater. 191–194 (1992) 942.
[14] H.M. Chung, L.J. Nowicki, J. Gazda, D.L. Smith, DOE/ER-0313/17, 1994, p. 211.
[15] H.M. Chung, B.A. Loomis, D.L. Smith, J. Nucl. Mater. 212–215 (1994) 804.
[16] M. Satou, K. Abe, H. Kayano, Ibid. p. 794.
[17] D.S. Gelles, H.M. Chung, DOE/ER-0313/21, 1996, p. 79.
[18] H.M. Chung, B.A. Loomis, D.L. Smith, J. Nucl. Mater. 233–237 (1996) 466.
[19] K. Fukumoto, H.M. Chung, J. Gazda, D.L. Smith, H. Matsui, Helium behavior in vanadium-based alloys irradiated in the dynamic helium charging experiments, Presented at the 18th ASTM International Symposium on Effects of Radiation on Materials, to be published.
[20] P.M. Rice, unpublished work.